

Influence of laser parameters on selective retinal treatment using single-phase heat transfer analyses

Rupak K. Banerjee^{a)}

Department of Mechanical Engineering and Department of Biomedical Engineering, University of Cincinnati, Cincinnati, Ohio 45221-0072

Liang Zhu

Department of Mechanical Engineering, University of Maryland Baltimore County, Baltimore, Maryland 21250

Pradeep Gopalakrishnan and Michael J. Kazmierczak

Department of Mechanical Engineering, University of Cincinnati, Cincinnati, Ohio 45221-0072

(Received 18 December 2006; revised 20 February 2007; accepted for publication 28 February 2007; published 26 April 2007)

Selective thermal treatment to retina is induced by short pulsed lasers to denaturize retinal pigment epithelium (RPE) selectively, while sparing the sensitive photoreceptors. The problem associated with the usage of short pulsed laser is the difficulty in determining the correct dosimetry parameters. This study quantifies the influence of laser parameters over the therapeutic range. The laser-tissue interaction is numerically investigated by analyzing the transient temperature in ocular tissues during the treatment. The rate process analysis for thermal injury is employed to estimate the selective damage of retina. The contours of Arrhenius integral value (Ω/Ω_{\max}) presented in this study show both the area and magnitude of damage caused by various laser parameters. Results reveal that the 2 μs pulsed laser with green wavelength and Gaussian profile is relatively more effective for selective retinal treatment. The repetition frequency of 100 Hz is found to produce selectively RPE damage, while higher frequencies produce collateral damage to neural retina and choroid located within 2 μm from the RPE interface. © 2007 American Association of Physicists in Medicine. [DOI: 10.1118/1.2718731]

Key words: laser therapy, selective retinal treatment, rate process analysis, retinal pigment epithelium

I. INTRODUCTION

Laser therapy to retina is used to treat a number of macular diseases such as age-related macular degeneration, diabetic maculopathy, central serous retinopathy, choroidal neovascularization, etc. Most of the macular diseases are related to the decline in retinal pigment epithelium (RPE) cell function. It has been suggested that cell proliferation and restoration of RPE barrier after the laser treatment enhances the pumping mechanism, which produces the clinical effects of reducing subretinal fluid and improving macular pathology.¹

During laser therapy, the photons are absorbed in the tissues, which results in the excitation or increase in energy of the molecules. The increase in energy leads to a rise in temperature, which breaks the weak bonds in protein, enzymes and, thereby causing denaturation of proteins. Many proteins are affected in the temperature range² of 50–80 °C. The degree of damage on a particular type of tissue depends on two factors, namely magnitude and duration of temperature increase. Similar tissue damage can be produced either by long exposure to low temperature or by short exposure to high temperature. This reciprocity between exposure duration and temperature is the critical factor, which helps in the development of selective retinal treatment (SRT). The SRT coagulates RPE selectively by short exposure to high temperatures.

The radiation parameters such as laser wavelength, profile, pulse width, and repetition frequency govern the magnitude of temperature rise and its duration.

Conventional laser treatment uses continuous wave (cw) laser with exposure time in the range of 100–200 ms, and power in the range of 50–200 mW. The laser is primarily absorbed by the melanin granules in the RPE tissue. Since the exposure duration is relatively long, the absorbed thermal energy spreads by heat diffusion into the neural retina and choroid, therefore, it may destroy the photoreceptors. The laser scar expands postoperatively and results in decrease in central visual sensitivity, epiretinal fibrosis, and reoccurrence of choroidal neovascularization. Alternatively, SRT uses short laser pulses, which minimizes the heat diffusion, localizes the thermal energy and hence spares the neural retina. Many previous experimental studies substantiated the possibility of producing SRT with pulsed lasers and analyzed the effect of laser parameters to enhance the selectivity, which is briefly reviewed below.

A. Influence of wavelength

Mainster^{2,3} studied the effect of wavelength based on absorption characteristics of melanin. Mainster conferred the undesirable effects of blue wavelength and the advantage of using green or red lasers. Further, Mainster recommended

selection of wavelength based on type and severity of disease; near infrared lasers are preferred over the visible lasers for severe subretinal hemorrhage, while visible laser are preferred for thin hemorrhage. However, many experimental studies³ showed that the selection of wavelength for conventional cw photocoagulation is not a critical factor for a better clinical outcome.

B. Influence of pulse width

SRT using 5 μs laser pulses with pulse energy in the range of 2–10 μJ at a repetition rate of 500 Hz was first carried out in rabbits by Roider *et al.*⁴ with 110 mm retinal spot size. They analyzed both the cw and pulsed lasers at various laser energies and exposure durations. They observed the proliferation of RPE cells after the SRT, at the periphery of lesion towards the center of the irradiated site. Further, they showed that it is impossible to produce selective damage by the cw laser, even with exposure durations in the order of a few milliseconds.

SRT in humans was performed by Roider *et al.*⁵ with 1.7 μs green laser at 500 Hz for a retinal spot diameter of 160 μm . The SRT disrupts RPE without producing ophthalmoscopically visible white or gray lesions. The white or gray lesion, formed during the cw photocoagulation, is due to the destruction of photoreceptors, which alters the scattering characteristics of the neural retina. They also showed effectiveness of SRT in treating the macular diseases like central serous retinopathy, drusen maculopathy, and diabetic maculopathy. Thus, it is evident that for these macular diseases, the therapeutic efficacy is associated with destruction of RPE and not with the destruction of photoreceptors. Autofluorescence imaging by Framme *et al.*⁶ after the SRT showed leakage from the irradiated site, proved the damaging of RPE by short pulsed lasers.

Influence of pulse width and pulse number was studied by Framme *et al.*⁷ with rabbits using 1.7 μs , 200 ns green laser at constant repetition rate of 100 Hz. They measured threshold energy, and energy required to produce 50% of the damage, for various pulse widths and pulse numbers. Their analysis was based on the safety margin factor, which is defined as the ratio of threshold energies required to produce 84% of angiographically visible lesion and 16% of ophthalmoscopically visible lesion. They showed high safety margin factors for short pulse width and high number of pulses.

C. Influence of repetition frequency

Roider^{8,9} and Brinkmann¹⁰ studied the primary interaction mechanism involved in nanosecond laser treatment. For pulse width in the range of microseconds, the threshold energy is proportional to $N^{-1/4}$, where N is the number of pulses. Effect of duty factor, defined as ratio of pulse-on time to the total pulse time, was studied by Berger¹¹ with a simplified two-dimensional model of the eye. They analyzed the thermal localization by comparing the temperature of RPE (T_{RPE}) to that of the deep choroid (T_{ch}). Comparison of cw with pulsed laser showed better localization (higher $T_{\text{RPE}}/T_{\text{ch}}$) for pulsed lasers with low duty factor (2%).

Mainster² discussed the additive effect for different duty factors and explained the temperature increase based on the $N^{-1/4}$ law. This study described lower irradiance requirement for higher frequencies, which leads to reduced thermomechanical damage and iatrogenic hemorrhage.

Summarizing the past literature above shows that, although there have been several experimental studies, the influences of laser parameters for retina are not well quantified owing to the difficulty in measuring the actual temperature during the photocoagulation. Furthermore, variation in thickness and melanin concentration of RPE contributes to error in experimental studies. Similar laser power could cause suprathreshold damage for heavy pigmentation, which produces damage to photoreceptors or could lead to subthreshold damage for low pigmentation, which does not produce the required therapeutic damage. Another important factor to be analyzed is the thermal diffusion after each laser pulse-on time, which can cause thermal damage to photoreceptors and choroid.

The current study is aimed at identifying the therapeutic range of laser parameters including wavelength, profile, pulse width, and repetition frequency by studying the temporal and spatial variations of temperature. Further, the impact of variation of melanin concentration over threshold energy requirement is analyzed. The selectivity of the treatment is analyzed using the rate process model for thermal damage, based on unimolecular chemical kinetics (discussed in detail in Sec. II E).

II. METHODOLOGY

A. Geometry

The geometrical description of the eye, given by Charles,¹² is used to create an axi-symmetric model of a complete eye as shown in Fig. 1(a). This model consists of nine different eye compartments: cornea, lens, iris, aqueous humour, vitreous humour, neural retina, RPE, choroid, and sclera. The thickness of neural retina, RPE, choroid and sclera are key parameters for the determination of correct laser heat source. The thickness of retina ranges from 500 μm near the optic nerve region to 50 μm near ora serrata.¹³ Similarly, the thicknesses of choroid and sclera have maximum values near the optic nerve and minimum values near the equator.^{13,14} Hence, the average thicknesses of 10, 190, 250, and 700 μm are used for RPE, neural retina, choroid, and sclera, respectively.¹⁵ The close-up view of RPE, neural retina and choroid regions is shown in Fig. 1(b).

B. Governing equation

The calculation of laser-tissue interaction is carried out by solving the following transient heat conduction equation, with temporal and spatial dependent laser heat source, throughout the various regions of ocular tissues using finite volume discretization technique

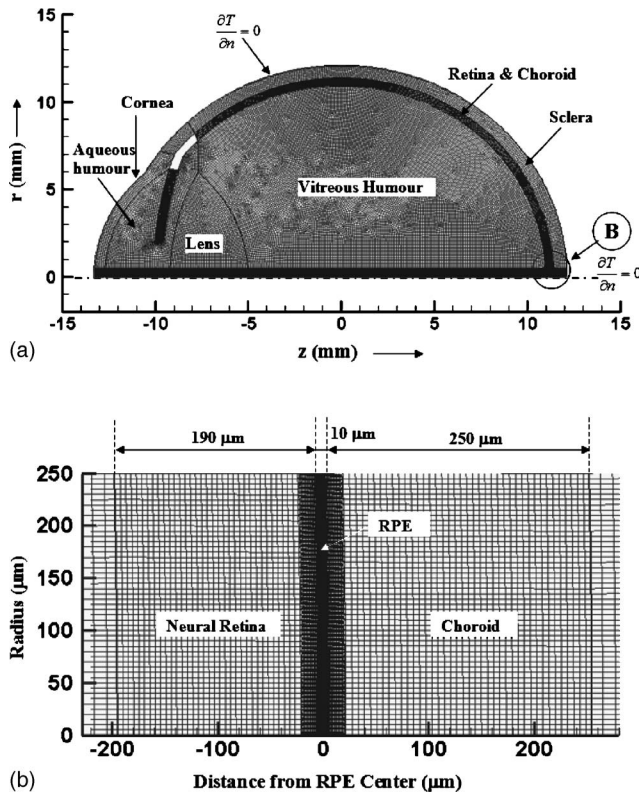


FIG. 1. Two-dimensional meshing of the eye model used in the present laser-tissue interaction study. (a) Axi-symmetric eye model. (b) Close-up view of area of interest.

$$\frac{\partial(\rho CT)}{\partial t} = \nabla \cdot (k \nabla T) + S(z, r, t), \quad (1)$$

where k is the thermal conductivity (W/m K), ρ is the density (kg/m^3), C is the specific heat capacity (J/kg K), and S is the volumetric laser source term (W/m^3), which varies spatially and temporally (discussed in detail in Sec. II D). A previous study [Welch *et al.*, 1980] has suggested that a very minor role is played by the local blood perfusion rate in tissue in laser treatment. Since the heating lasts less than 1 s, the effect of local blood perfusion is neglected in the study.

In a normal eye, vitreous flows through retina at a flow rate of $0.14 \mu\text{L}/\text{min}$.¹⁶ In order to delineate possible cooling effect by the vitreous, an initial computation is conducted by including convection terms in the governing equation. The

comparison of results with no convection shows that the temperature rise remains unaffected by vitreous outflow. This is due to the low flow rate of vitreous and short duration, few hundred milliseconds, of the laser photocoagulation. Hence, the convection due to ocular hydrodynamics is neglected for all the results presented in this study.

Thermo-physical properties of each ocular structure are critical for the evaluation of actual temperature elevation during laser therapy. The properties of ocular tissues based on a previous study¹³ are given in Table I. The value of thermal conductivity of choroid is unavailable in the literature. In this study, we assume that its thermal properties are similar to that of the retina, based on the assumption that water is the major component of both tissues.

C. Heat source distribution

The heat generation rate due to laser-tissue interaction depends on two parameters, namely, the fluence rate and the absorption coefficient. It is given by

$$S(r, z, t) = \mu_a(z) \phi(r, z), \quad (2)$$

where μ_a is the absorption coefficient, which depends on type of tissue and incident laser wavelength, λ , and $\phi(r, z)$ is the fluence rate (W/m^2). The fluence rate depends on many parameters, including laser intensity, spot diameter, and optical properties of tissues such as scattering and absorption. If absorption dominates scattering ($\mu_a \gg \mu_s$), the fluence rate is governed by the Beer-Lambert law as

$$\phi = \frac{I_0}{\pi R^2} \exp(-\mu_a z) \quad \text{for } \mu_a \gg \mu_s, \quad (3)$$

where R is the radius of laser spot (m), I_0 is the incident laser power (W) and z is the depth of the irradiated material (m). For materials whose scattering is of the order of absorption, the fluence rate predicted by the Beer-Lambert law may not be accurate.^{17,18} Welch¹⁷ developed an alternative fluence rate based on combined scattering and absorption characteristics. They suggested the fluence rate for considerable scattering as

$$\phi = \frac{I_0}{\pi R^2} \exp[-(\mu_a + (1-g)\mu_s)z] \quad \text{for } \mu_a \sim \mu_s, \quad (4)$$

where g is the anisotropy factor, which is the cosine of average scattering angle. Since ocular tissues possess highly forward scattering characteristics (anisotropy factor, g , ranges from 0.85 to 0.97), the assumption holds good for

TABLE I. The values of the thermo-physical properties of ocular tissues used in the numerical computations.

Properties	Vitreous Humor ^a	Retina ^a	Choroid	Sclera ^a
Thermal conductivity (W/m K)	0.603	0.628	0.628	0.58
Density (kg/m^3)	1000	1000	1000	1050
Specific heat capacity (J/kg K)	4178	4190	4190	4178

^aReference 13.

TABLE II. The values of optical properties of ocular tissues for green, red and infrared laser.

Ocular tissue	Wavelength λ (nm)	Absorption μ_a (m^{-1})	Scattering μ_s (m^{-1})	Anisotropy factor g	$\mu_a + (1-g)\mu_s$
Neural retina	527 (green)	0.421	34.188	0.97	1.45
	650 (red)	0.125	25.254	0.97	0.88
	810 (infrared)	0.069	21.866	0.97	0.72
RPE	527	110.243	114.637	0.84	128.58
	650	84.063	123.161	0.84	103.77
	810	41.570	162.126	0.84	67.51
Choroid	527	15.939	73.587	0.87	25.51
	650	8.626	57.363	0.87	16.08
	810	4.288	51.188	0.87	10.94
Sclera	527	0.411	89.827	0.9	9.39
	650	0.202	68.272	0.9	7.03
	810	0.032	50.617	0.9	5.09

ocular tissues. In order to predict the accurate heat source values, the scattering and absorption characteristics of all ocular tissues, namely vitreous humour, neural retina, RPE, choroid and sclera are incorporated. The values of μ_a , μ_s and anisotropy factor g (Table II) are taken from the *in vitro* results by Hammer.¹⁹ They employed double-integrating sphere technique and inverse Monte Carlo simulation to calculate the optical properties of ocular tissue. In this study, an anisotropy factor of 84% is used for RPE and the energy scattered in the direction other than the direction of the laser beam is ignored. Hence, the scattering coefficient has an appreciable effect on the heat source distribution, as shown in Table II. Further, since there were no previous experimental studies of the exact value of scattering coefficient, we used the values reported in Hammer.¹⁹

The variation of laser intensity along radial direction depends on the profile of the beam. For top-hat profile, i.e., uniform intensity along radial direction, the heat source for a particular ocular tissue is

$$S(z, r, t) = \delta_{\text{on}} \frac{I_0 \mu_a(z)}{\pi R^2} \exp[-(\mu_a + (1-g)\mu_s)z], \quad (5)$$

where δ_{on} is a multiplication factor used to simulate pulsed laser, which has a value of one or zero corresponding to on and off duration, respectively. For Gaussian profile, variation of incident intensity along the radial direction is also included as follows:

$$S(z, r, t) = \delta_{\text{on}} \frac{2I_0 \mu_a(z)}{\pi R^2} \times \exp[-(\mu_a + (1-g)\mu_s)z] \cdot \exp\left(\frac{-2r^2}{R^2}\right), \quad (6)$$

where r is the radial distance from the central line of the laser path in cylindrical coordinate system (m).

D. Boundary conditions

Thermal boundary conditions are required on all sides of the domain to solve the heat diffusion equation. At the axis zero heat flux condition (symmetry) is imposed:

$$\frac{\partial T}{\partial r} = 0 \quad (\text{along the axis}). \quad (7)$$

The actual boundary conditions at the ends of sclera and cornea are unknown. In previous numerical analysis by Amara,¹³ convective heat transfer or mixed-type boundary conditions were used at the ends of sclera and cornea. Further, Amara has analyzed the effect of boundary conditions by applying a wide range of convection heat transfer coefficients. The results showed the insignificant effect of boundary conditions over the solution. This is because of the significant difference in length scale associated with the eye geometry (in mm) and the size of the laser spot (in μm). Moreover, since total time exposure is in the range of a few

TABLE III. The value of pre-exponential factor and activation energy E_a for different temperatures used in the present study to compute the Arrhenius integral value Ω .

Reference	Temperature range (K)	Pre-exponential factor A (s^{-1})	Activation energy E_a (J/mole)
Takata <i>et al.</i> ^a	≤ 316	0	
	$316 < T \leq 323$	4.3×10^{64}	4.2×10^5
Bringruber, Hillenkamp and Gabel ^b	$323 < T$	10^{44}	2.93×10^5

^aReference 23.

^bReference 21.

TABLE IV. Summary of runs. Case 1 is the validation of temperature with experimental results. Case 2 serves as the reference base line case. Laser parameters (in bold) are varied as shown in runs 3–9 to show their influence over the selectivity of the treatment.

Runs		λ (μm)	Profile	Δt_p (μs)	Energy /pulse (μJ)	Repetition frequency (Hz)	n	Exposure duration (ms)	Average power (mW)
1	Validation	527	Top hat	1.7	100	100	30	300	10
2	Base case	527	Top hat	2	22.5	500	50	100	11.25
3	λ	650	Top hat	2	24	500	50	100	12
4		810	Top hat	2	42	500	50	100	21
5	Profile	527	Gaussian	2	14	500	50	100	7
6	Δt_p	527	Top hat	20	25	500	50	100	12.5
7		527	Top hat	200	30	500	50	100	15
8	Repetition	527	Top hat	2	30	100	50	500	3
9	Frequency	527	Top hat	2	16	1000	50	50	16

hundred milliseconds, the domain behaves as infinite length in the z direction.

In order to validate the applicability of the boundary condition, as an initial step, two limiting boundary conditions, i.e., constant temperature (Dirichlet B.C.) and zero heat flux (Neumann B.C), are analyzed. The maximum temperature obtained by the two cases differs only by 0.02%. Thus, the zero heat flux boundary condition is applied for all calculations presented in this study

$$\frac{\partial T}{\partial n} = 0 \text{ (along the periphery of sclera and cornea).} \quad (8)$$

E. Rate process analysis of thermal damage

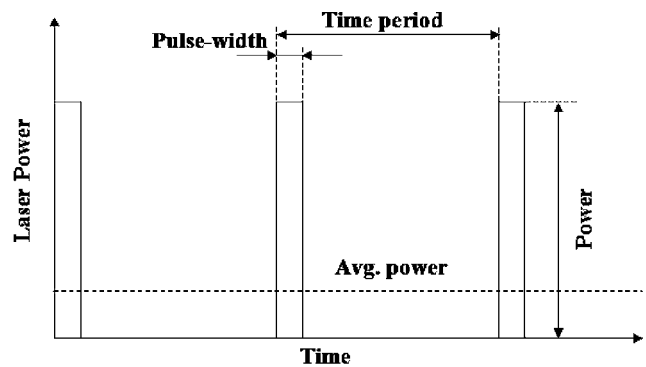
The rate process analysis for thermal damage was first reported by Moritz and Henriques.²⁰ In their work, thermal damage to tissue at time t was quantified using a single parameter, Ω , which is calculated from an Arrhenius integral as follows:

$$\Omega(t) = A \int_0^t \exp[-E_a/R_u T(t)] d\tau, \quad (9)$$

where A is the frequency or pre-exponential factor (1/s), E_a is the activation energy barrier (J/mole), R_u is the universal gas constant (8.32 J/mole K) and T is the absolute temperature (K). The effect of both magnitude and duration of temperature increase is included in the Arrhenius integral value (Ω), as it involves integration of temperature over time. Thus, the value of Ω is a measure of the accumulative thermal damage caused by the laser treatment.

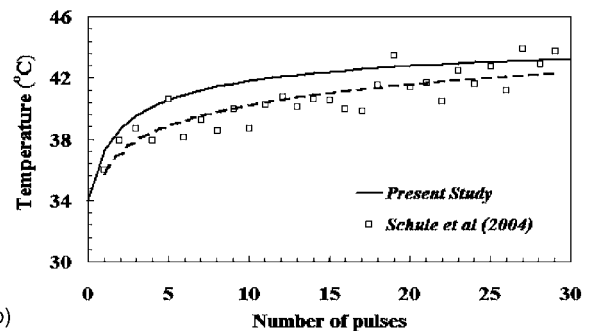
The rate process model of thermal damage is based on first-order unimolecular chemical kinetics. Detailed derivation of the rate process model has been described in many earlier studies.^{17,20–22} The values of E_a and A for laser treatment were measured by many previous experimental studies.²² Welch¹⁸ showed that the activation energy remains constant for a wide range of temperatures, while the pre-exponential factor increases with temperature. The activation energy and the frequency factor of retina for different tem-

perature ranges used in this study are shown in Table III. Experimental results by Takata²³ showed that the temperature rise of up to 6 °C produces negligible damage and hence zero value is used for pre-exponential factor A for temperatures less than 316 K. An experimental investigation by Bringruber²¹ was conducted at a temperature of 350 K.



$$\begin{aligned} \text{Energy/pulse} &= \text{Power} * \text{Pulse-width} \\ \text{Frequency} &= 1/ \text{Time period} \\ \text{Exposure Duration} &= \text{No. of pulse} * \text{Time period} \\ \text{Avg. power} &= \text{Energy/pulse} / \text{Time period} \end{aligned}$$

(a)



(b)

Fig. 2. Comparison of base line temperature (lowest temperature at the end of each pulse) of present results with experimental results by Schule *et al.* (2004). The laser parameters are: wavelength—green, profile—top-hat, pulse width—1.7 μs , energy/pulse—100 μJ , frequency—100 Hz, number of pulses—30, spot diameter—160 μm .

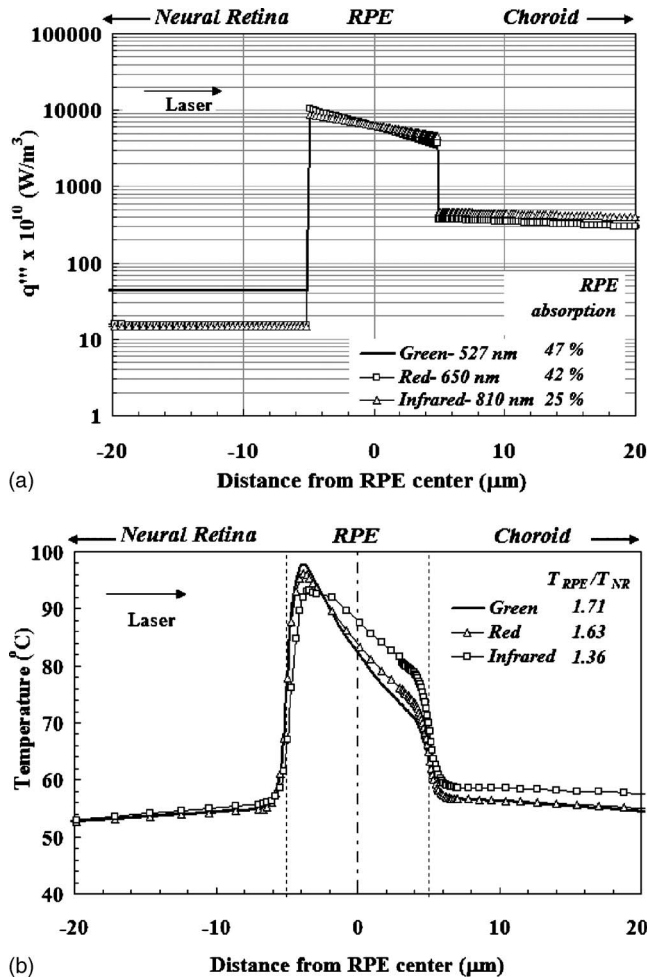


FIG. 3. Comparison of source profiles and resulting temperatures for all three wavelengths (527, 650, 810 nm). (a) Variation of laser heat source profiles along the depth. The regions of neural retina, RPE and choroid are shown in the graph. The green wavelength has high absorption in all three layers followed by the red and infrared rays. (b) Predicted maximum temperature along the centerline of the laser beam.

We assume in the present numerical study the values of E_a and A from Bringruber²¹ are applicable to temperatures above 323 K. Trapezoidal rule is employed to compute the value of Ω [Eq. (9)] and the mean temperature is used to select the values of E_a and A .

F. Finite volume method

The finite volume mesh is generated in Gambit 2.1.0 using the Cooper scheme with $\sim 60,000$ cells of quadrilateral elements. Heat conduction equation is solved using finite volume method. Double precision coupled solver with second-order time implicit scheme is employed to discretize the governing equations. A second-order upwind scheme is adapted for the energy equation. Convergence criterion for the energy equation^{24,25} is kept at 10^{-6} , which is an order of magnitude lower than recommended values. Mesh independence is checked by increasing the number of elements in the RPE region by 20% over the current mesh and both the results are compared. The finer mesh showed less than 1%

difference in temperature. For detailed numerical technique on finite volume method, our earlier publications^{24,25} on laser and x-ray heating may be referred to.

III. RESULTS

The success of selective retinal photocoagulation depends primarily on the laser parameters. The results from this study quantitatively show the influence of laser parameters such as wavelength, laser profile, pulse width, repetition frequency on the selective damage of RPE. The summary of different computations performed is listed in Table IV.

A base line computation (case 2) is carried out with the following laser parameters: wavelength λ —527 nm (green), profile—top-hat, pulse width Δt_p —2 μs , energy/pulse—22.5 μJ , frequency f —500 Hz, and number of pulses n —50, exposure duration—100 ms and average power—11.25 mW. The spot diameter of 100 μm is kept the same in all computations.

The effects of laser parameters are studied by varying the corresponding values (Table IV) from the base line case. The transient temperature and the Arrhenius integral value, Ω , are obtained from the cases. The temperature profile along the center of the laser is analyzed to study the deposition and diffusion of thermal energy. The ratio of maximum temperature at the RPE (T_{RPE}) to the temperature at the neural retina (T_{NR}), 5 μm away from the RPE-neural retina interface, is used to quantify the “selectivity.” The energy/pulse for each case is varied in order to achieve an Ω value of near 1 (Table IV). Since Ω is a highly nonlinear function of temperature, it is not trivial to obtain a specific value, e.g., a unique value of 1, at a particular location for all laser parameters. Though the order of magnitude of Ω_{max} is ~ 1 , it differs from one case to another. Thus, using the new value of Ω_{max} for each case, further normalization of contours $\Omega/\Omega_{\text{max}}$ is necessary for improving comparison of the effects of laser parameters on thermal damage. Since the Ω_{max} value for all runs is ~ 1 , the contour plots show comparable magnitude and area of damage. A higher value $\Omega/\Omega_{\text{max}}$ at neural retina signifies more damage to the photoreceptors, while a lower value represents selective damage of RPE.

A. Validation

The definition of laser parameters used in the study such as energy/pulse, repetition frequency and average power, in terms of pulse width and pulse power, are given in Fig. 2(a). The results of this present calculation are validated with the *in vivo* temperature measurements taken by Schule²⁶ using optoacoustic methods. They conducted an experiment by applying 30 pulses of 1.7 μs green laser at 100 Hz with 100 μJ pulse energy. The base line temperature, defined as temperature at the end of each pulse-off cycle, was measured during the treatment. The calculation for the present study is conducted with the same laser parameters (Table IV: case 1) with initial temperature of 34 $^{\circ}\text{C}$. Figure 2(b) shows the variation of the base line temperature with number of pulses for experimental²⁶ and present study. A log-fit curve to the experimental result is also shown in Fig. 2(b). The tempera-

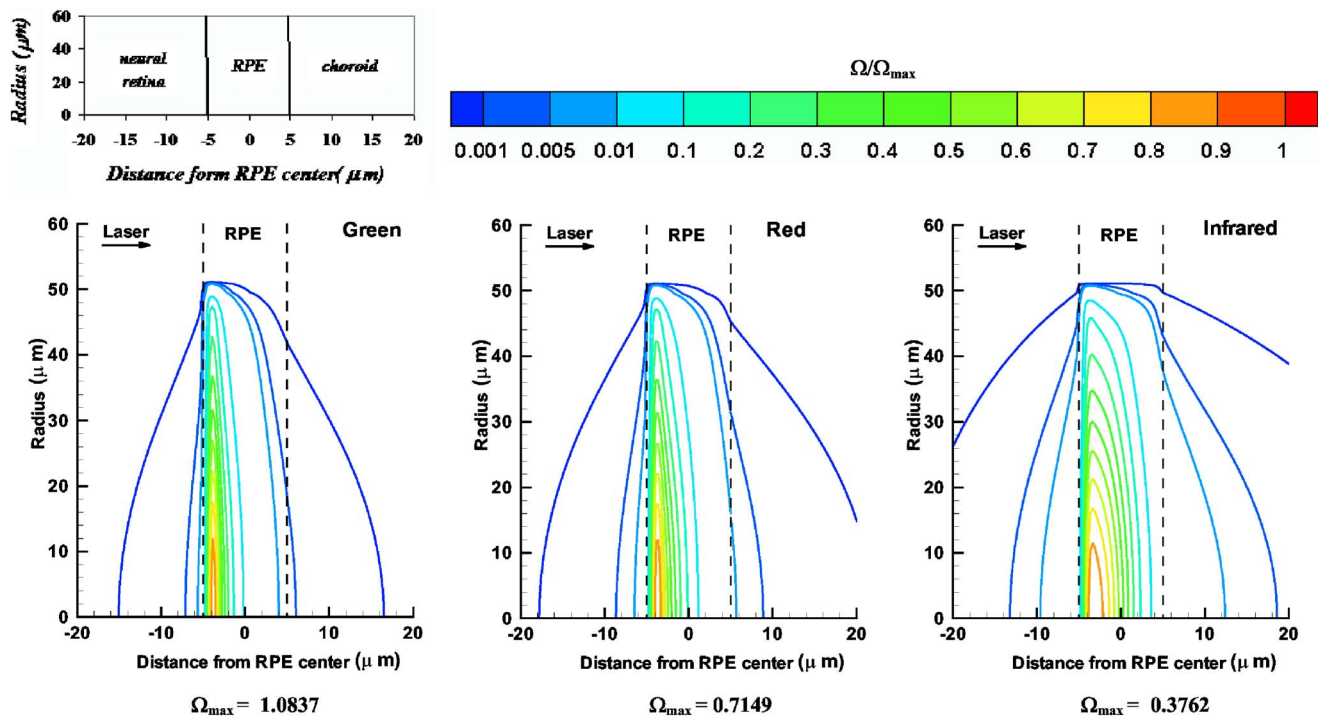


FIG. 4. Contours of Ω/Ω_{\max} for all three wavelengths at the end of 50 pulses. For the same laser power, the green wavelength produces maximum damage to RPE (high Ω_{\max}), while infrared produces minimum damage. The contours of red and infrared rays show damage to neural retina and choroid.

ture predicted by present study is higher than the experimental study and the average deviation is 3.5% and maximum deviation is within 8%. The deviation may be due to local variation of RPE thickness and melanin concentration. Further, the experimental results²⁶ have a standard deviation of 17% due to the usage of material constants of porcine RPE.

B. Effect of wavelength

The melanin granules in RPE have strong absorption characteristics for wavelengths in the visible range, and its absorption decreases with increase in wavelength. The influence of wavelength is studied by analyzing three frequently used wavelengths (Table IV: cases 2, 3, and 4) namely green (527 nm), red (650 nm), and infrared (810 nm). The absorption coefficient of RPE for red and infrared lasers is lower than that of green laser. Hence, the energy/pulse for red and infrared lasers is increased from 22.5 of the base case to 24 and 42 μJ , respectively, in order to obtain an Ω value of around 1. The thermal energy deposited as depicted by the heat source profiles given by Eq. (5) is shown in Fig. 3(a). For all the three wavelengths, the heat generation is high in RPE and few orders of magnitude lower in neural retina and choroid. The main advantage of green laser is the high absorption $\sim 47\%$ of incident energy in RPE, while it is $\sim 42\%$ and $\sim 25\%$ for red and infrared rays, respectively. The advantages of red and infrared rays over green rays are that the value of heat source at the interface of RPE and neural retina is low and absorption in the neural retina is significantly less than that of green rays.

Figure 3(b) shows comparison of the resulting temperatures at the end of the 50th pulse along the center of the laser

beam. The green laser produces temperature of around 98 °C at RPE, while infrared produces a temperature of 94 °C. Although green laser results in higher energy absorptions in both the RPE and neuro retina layers than either red or infrared laser, the enhancement in the green laser absorption is significant in the RPE, while it is modest in the neuro retina layer. Therefore, one notes a higher ratio of $T_{\text{RPE}}/T_{\text{NR}}$ for green laser. The value of $T_{\text{RPE}}/T_{\text{NR}}$ is 1.74 for green, 1.70 for red, and 1.59 for infrared laser. The higher temperature ratio implies relatively better selective damage of the RPE.

Contours of Ω/Ω_{\max} for three wavelengths are shown in Fig. 4. Since Ω_{\max} value for all runs is ~ 1 (near 1), these contours show both area and level of damage. The actual value of Ω can be obtained by multiplying the contour value with Ω_{\max} , which is also shown in the figure. The location of RPE is from -5 to $+5 \mu\text{m}$. The contours for green wavelength show that the thermal damage is limited to RPE, as the value of Ω/Ω_{\max} is 0.01 at neural retina and choroid. The contours of red and infrared show the significant damage beyond RPE to neural retina and choroid. The value of Ω/Ω_{\max} at neural retina is 0.1 and 0.3 for red and infrared lasers, respectively. Hence, despite the advantage of a low heat source at interface of RPE-neural retina and lower absorption in neural retina, the red and infrared produces thermal damage to neural retina. Thus, the fraction of energy absorbed in the RPE is the main criteria for selectivity of the treatment.

Further, the threshold energy required for green laser is lower than that of red and infrared rays. Another important factor to be considered is the amount of transmitted energy (unabsorbed laser energy leaving the sclera), as higher trans-

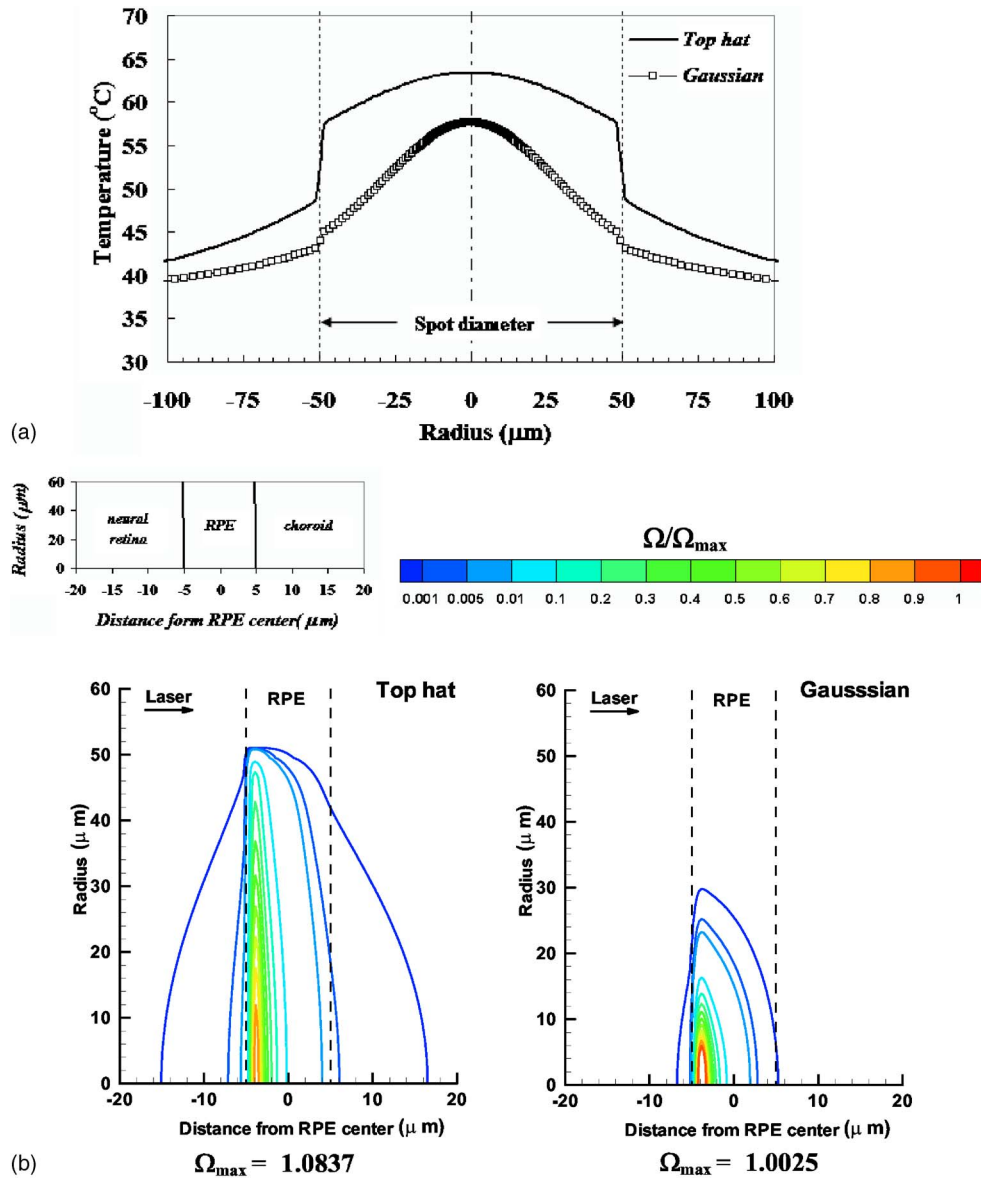


FIG. 5. Comparison of temperature and Ω for Gaussian and top-hat laser beam profiles. (a) Temperature along radial direction at the end of 50 pulses. Gaussian profile results in high temperature at the center of the beam. (b) Contours of Ω/Ω_{\max} for Gaussian and top-hat profile. The contours of Gaussian profile show selective damage along the radial direction.

mission may be the result in postoperative complications. For green laser almost 70% of incident energy is absorbed, whereas it is 65% and 50% for red and infrared rays, respectively. Thus, based on selective effect, lower threshold energy requirement, and transmission criteria, the green laser is preferred over red and infrared lasers.

C. Effect of laser beam profile

The intensity pattern of laser along radial direction depends on the transverse electro-Magnetic (TEM) operating mode of the laser. The fundamental mode (TEM00) produces a Gaussian profile, while the multimode produces a near uniform intensity profile (top hat), over the spot diameter. In this study, the effect of the laser profile on the therapeutic effect

is analyzed by comparing computations with two different laser profiles: Gaussian and top hat (Table IV: cases 2 and 5). The energy/pulse of Gaussian profile is reduced to 14 μJ to result in a similar Ω_{\max} .

Figure 5(a) shows resulting temperature along the radial direction at the end of the 50 pulses for two profiles. The Gaussian profile produces a temperature of $\sim 55^\circ\text{C}$ at the center of the beam, while the top-hat profile produces a temperature of $\sim 60^\circ\text{C}$. Since the intensity of Gaussian profile is low near the edge of the laser spot, it produces lower temperatures outside the laser spot. The contours of Ω/Ω_{\max} for the two profiles are shown in Fig. 5(b). The contour for the beam with the Gaussian profile show selective damage in the radial direction. Since the Gaussian distribution requires

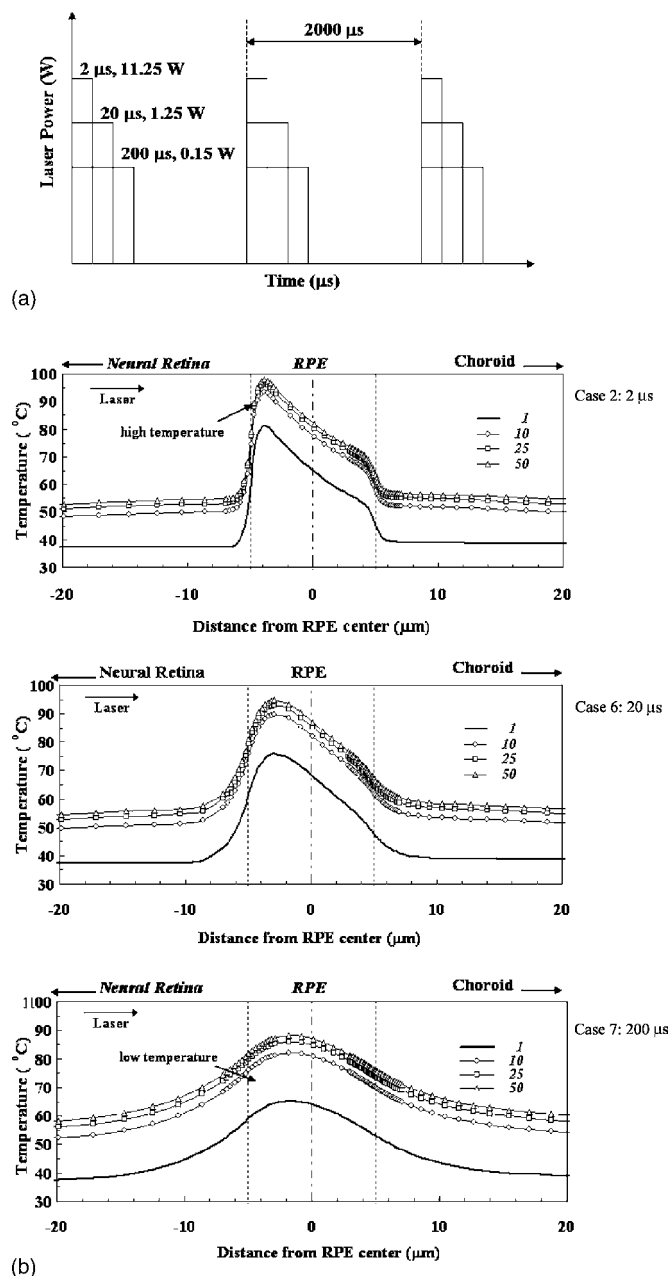


FIG. 6. Comparison of laser power and temperature for all three pulse widths 2 μs (Case 2), 20 μs (Case 6), and 200 μs (Case 7). (a) variation of pulse power and pulse-off duration with pulse width, (b) temperature along the centerline of the beam at the end of 1, 10, 25, 50th pulse for all pulse widths. The maximum temperature augmentation occurs within ten pulses and further increase in number of pulses does not produce significant additional temperature rise.

lower threshold energy than top hat and it produces selective damage along the radial direction, it is preferable to that of top hat.

D. Effect of pulse width

The effect of pulse width in selective damage was successfully demonstrated by a number of experiments.⁴⁻⁷ The main supporting argument for the selection of short-pulsed laser is that it reduces the thermal diffusion to the surround-

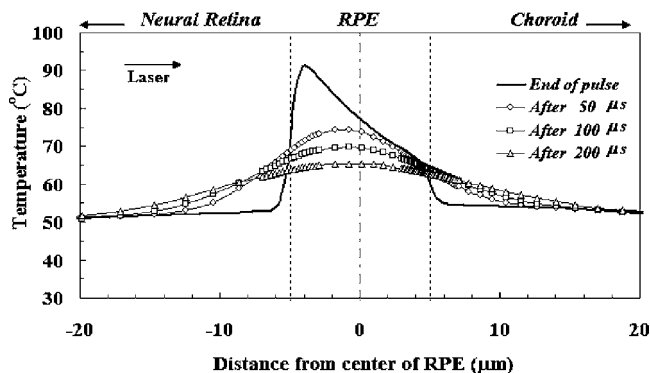


FIG. 7. Spreading of deposited energy after the pulse-on period for 2 μs laser treatment. The temperature of neural retina increases to 65 $^{\circ}\text{C}$ at 50 μs after the end of 50 pulses.

ing tissue, and thus, causes selective damage of RPE. However, the energy diffusing after the pulse-on can increase the temperature of neural retina and choroid. The current study evaluates the effectiveness of short-pulsed laser in terms of temperature and the Arrhenius integral value.

Three pulse widths 2, 20, and 200 μs (Table IV: cases 2, 6, and 7) are analyzed in this study. The energy/pulse of 20 and 200 μs pulses is increased to 25 and 30 μJ in order to compensate for diffusion losses. The variation of laser power and the pulse-off duration for all pulse widths are shown in Fig. 6(a). The temperature profiles along the central axis at the end of different number of pulses are shown in Fig. 6(b). For all pulse widths, the maximum temperature is nearly achieved within the first ten pulses and only moderate temperature rise occurs between the tenth and 50th pulses. For 2 μs pulse, there is no significant conduction occurring during the pulse-on duration and thus, the thermal energy is confined to the RPE. This, in turn, results in minimum temperature of $\sim 50^{\circ}\text{C}$ at the neural retina for 2 μs pulse. In case of 200 μs pulse width, higher thermal diffusion of energy into neural retina is observed. This results in higher temperature of $\sim 70^{\circ}\text{C}$ in a significant portion (till $\pm 5 \mu\text{m}$) of the neural retina.

The diffusion after the end of the 2 μs pulse-on duration is studied by analyzing the transient temperature profiles along the center axis at different times after the 50th pulse. Figure 7 shows a temperature increase in neural retina and choroid from 50 to 65 $^{\circ}\text{C}$ at around 50 μs after the end of the 50th pulse. Thus, even for 2 μs pulse width, diffusion after the pulse increases the temperature of neural retina. However, the temperature drops from 65 to 60 $^{\circ}\text{C}$ at around 200 μs after the end of the 50th pulse. As mentioned earlier, the damage depends on both magnitude and duration of temperature increase. Thus, the value of Ω needs to be analyzed to find selectivity of the treatment.

Figure 8 shows contours of $\Omega/\Omega_{\text{max}}$ for all pulse widths. The values of Ω_{max} are 1.0837, 0.8593, and 0.5929 for 2, 20, and 200 μs , respectively. The $\Omega/\Omega_{\text{max}}$ contours for 200 μs show the significant damage to neural retina and choroid and the value of $\Omega/\Omega_{\text{max}}$ is 0.3 at neural retina. For 20 μs pulse width, the damage occurs till $\pm 5 \mu\text{m}$ from the interface of

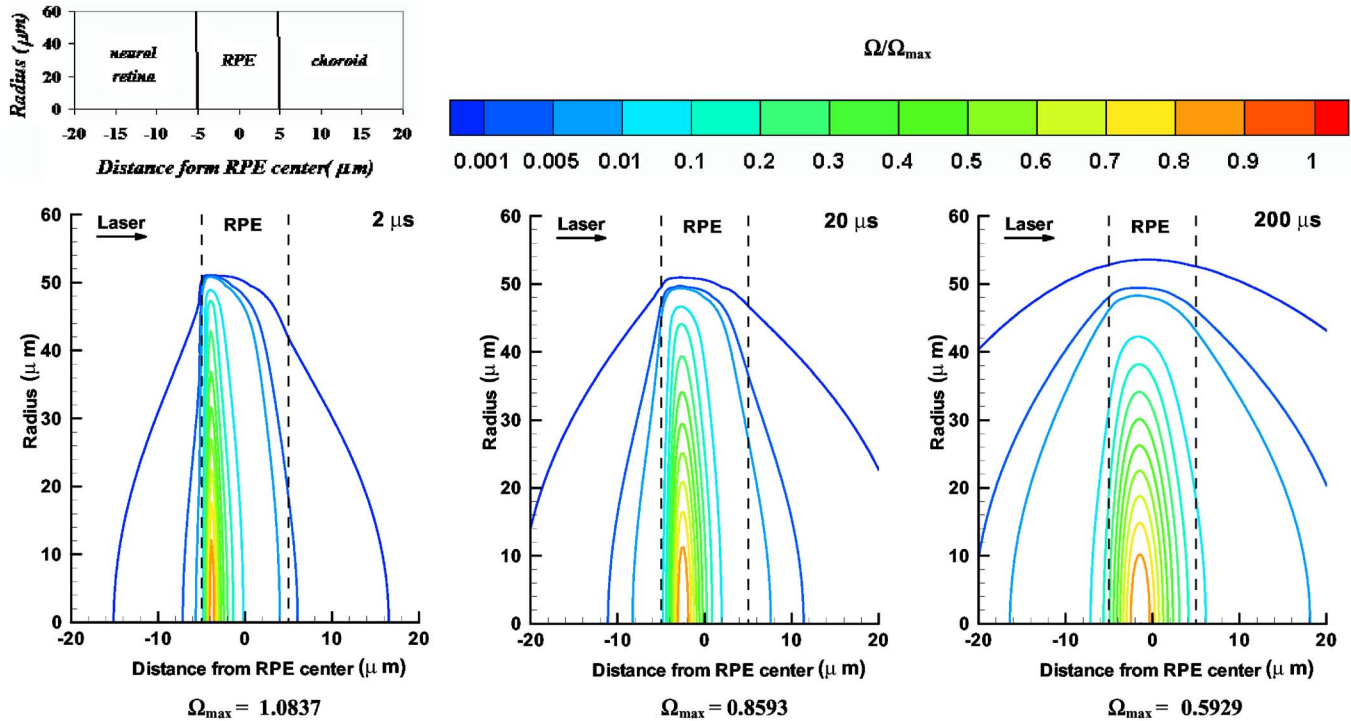


FIG. 8. Contours of Ω/Ω_{\max} for all pulse widths 2, 20, and 200 μs . The damage to neural retina and choroid is significant in the cases of 20, 200 μs , while the 2 μs produce selective RPE damage.

RPE-neural retina. For 2 μs , the damage occurs only to the RPE and the value of Ω/Ω_{\max} is around 0.01 in the neural retina and choroid regions. Thus, despite the temperature rise in the neural retina after the pulse-on, the 2 μs pulse produces selective damage. This is due to high temperature at RPE [Fig. 6(b)] and short duration of temperature increase in neural retina (Fig. 7). The short-pulsed laser effectively produces selective damage to the RPE, sparing the neural retina and choroid.

E. Effect of repetition frequency

The repetition frequency or duty factor is another important parameter in selective retinal photocoagulation treatment. Previous studies by Mainster² used repetition frequency in the range of 100–1000 Hz. In this study, the influence of repetition frequency is analyzed by simulating three cases (Table IV: cases 2, 8, and 9) with repetition frequencies of 100, 500, and 1000 Hz. In all the cases, 50 pulses of 2 μs pulse width are used. The energy/pulse for 100 and 1000 Hz is changed based on $N^{-1/4}$ law (N - number of pulses) to 30 and 16 μJ , respectively. Figure 9(a) shows the variation of pulse-off duration and average power for all repetition frequencies.

The transient temperature at the center of RPE for all frequencies is shown in Fig. 9(b). The maximum temperature at the end of each pulse remains the same for 100 Hz

and does not show any cumulative effect, while the high frequency 1000 Hz shows a strong cumulative effect in the temperature increase. In case of 100 Hz, the pulse-off cycle duration is sufficiently long, so that the temperature of RPE drops to the initial temperature before the next pulse cycle. For 1000 Hz, the pulse-off cycle duration is much shorter, and does not allow enough time for dissipation of thermal energy in the interim period. This results in augmentation of thermal energy and cumulative increase in temperature to a value of $\sim 95^\circ\text{C}$ in RPE at the end of the 50 pulses.

Figure 10 shows the temperature for all three frequencies along the centerline of the laser beam after 50 pulses. The maximum temperature of 100°C occurs at RPE for all repetition frequencies. The frequency of 100 Hz produces lower temperature of 40°C at neural retina, while a temperature of 65°C is obtained for 1000 Hz. The value of $T_{\text{RPE}}/T_{\text{NR}}$ is high 2.30 for 100 Hz pulse and it is 1.50 for 1000 Hz. Thus, high frequencies result in relatively increased diffusion of thermal energy to the neural retina due to less dissipation of energy during pulse-off duration.

Figure 11 illustrates the Ω/Ω_{\max} contours for all repetition frequencies. The frequency of 100 Hz shows selective damage to the RPE, while frequencies of 500 and 1000 Hz show damages to neural retina and choroid. The Ω_{\max} values are 1.7082, 1.0837, and 0.9640 for 100, 500, and 1000 Hz, respectively. It is evident from the contours that the area of damage increases as repetition frequency increases. The Ω/Ω_{\max} value of 0.3 at neural retina is obtained for 1000 Hz.

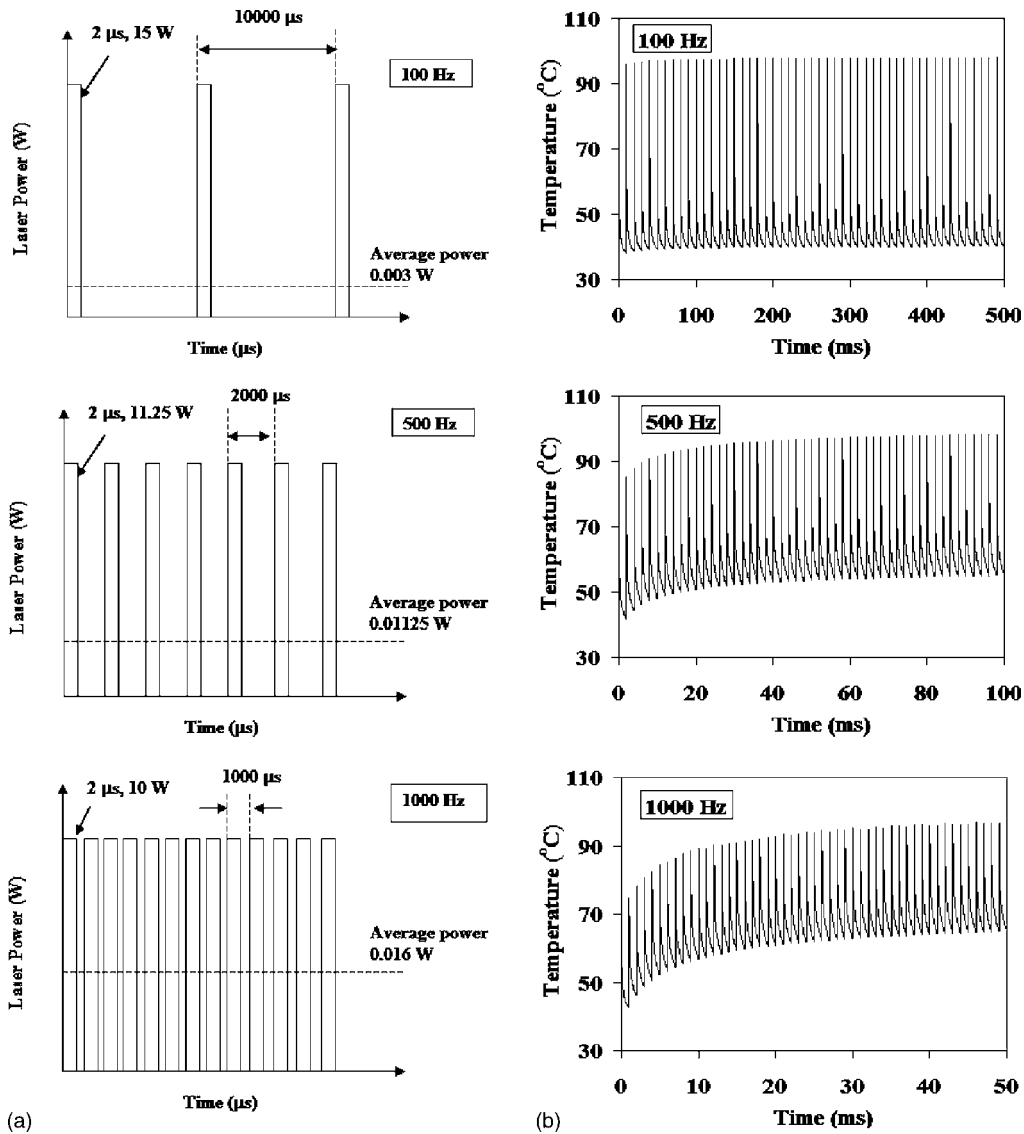


FIG. 9. Comparison of laser power and temperature for all for repetition frequencies of 100, 500 and 1000 Hz. (a) Variation of pulse-off duration and average power with repetition frequency. Same energy/pulse of 10 μJ is used for all repetition frequencies. (b) Transient temperature rise for all frequencies. The frequency of 1000 Hz shows strong cumulative effect in temperature with number of pulses, while frequency of 100 Hz shows the same temperature at the end of each pulse.

Hence, based on temperature and Ω/Ω_{\max} contours, the repetition frequency of 100 Hz produces selective damage with a low threshold energy requirement.

IV. DISCUSSION

The knowledge of accurate temperature increase during SRT is critical for the evaluation of therapeutic efficacy of the treatment. Present numerical study predicts the temperature during SRT for various laser parameters. The heat source, caused by the laser-tissue interaction, is modeled by three important optical properties of tissues, such as, absorption coefficient, scattering coefficient, and anisotropy factor. Further, unimolecular chemic kinetics is employed to find a measure of total thermal damage (Arrhenius integral value Ω) caused during pulsed-laser treatments. In addition to temperature, the present work compares the Arrhenius integral

value Ω for various laser parameters. One advantage of the current model is to identify a combination of laser parameters to achieve a maximum Arrhenius integral around 1 at the RPE, therefore, to evaluate thermal damages in different regions. Contours of Ω/Ω_{\max} are plotted for the RPE, neural retina, and choroid regions (Figs. 4, 5(b), 8, and 11) for assessing collateral damage to the vicinity of the RPE. These contours show both the area and the magnitude of the damage caused during the treatment, which demonstrates the influence of laser parameters on the selectivity value.

The present study illustrates the beneficial effect of green ray over the red and infrared rays for short-pulsed lasers. The green laser has high absorption in neural retina and high value of heat source at the interface of RPE and neural retina. Despite these disadvantages, the Ω/Ω_{\max} contours show a low value of 0.01 at the neural retina for green and higher

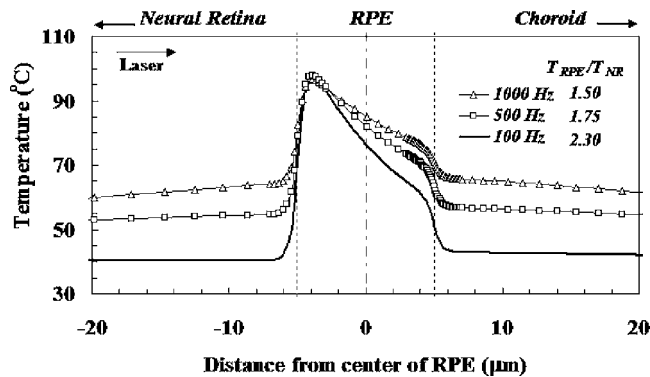


FIG. 10. Temperature along the centerline of the laser beam for all repetition frequencies at the end of 50 pulses.

values of 0.1 and 0.3 for red and infrared rays, respectively. Further, the present study validates the effectiveness of short pulsed laser in minimizing the damage to neural retina. Even though the temperature of neural retina increases for $2 \mu\text{s}$ case due to the diffusion of stored thermal energy from RPE, the short-pulsed laser show minimum damage ($\Omega/\Omega_{\text{max}} = 0.01$) to neural retina. The spot diameter is held at $100 \mu\text{m}$ for all the cases present in this study. The variation of spot diameter will have an impact over the selection of repetition frequency and the pulse width. Hence, further study with different spot diameter in conjunction with repetition frequency is required to find complete range of laser parameters required for the selective damage of RPE.

Unlike laser photocoagulation of small blood vessels in other laser treatments, significant water vaporization and explosion in blood are not considered in the current model. Blood vessels are present in the neural retina and choriocapillaris in the eye. In a previous theoretical simulation of temperature field during laser therapy for port wine stain [Jia *et al.*, 2006], 108°C was selected as the temperature at which water vaporization occurs. This temperature is much higher than the maximum temperatures in both the neural retina and choroid when the maximum Ω is kept around 1. Therefore, the current model may still be accurate in assessing the thermal transport in the RPE and its vicinity.

The limitation of this study is that the laser-tissue interaction is assumed to cause uniform heat source in the RPE. The laser is mainly absorbed by melanin granules of RPE and then energy diffuses to the neighboring cells. The melanin granules have a diameter of about $0.5 \mu\text{m}$, and are separated by mean distance of $1.2 \mu\text{m}$.²¹ The time required to reach uniform heat source by diffusion is around $1-2 \mu\text{s}$. Further, Brinkmann *et al.*¹⁰ showed that the local melanin granules temperature depends on both density of melanin granules and the pulse duration. They showed that the temperature of single melanin increases by a factor of 3 when pulse duration is changed from microsecond to nanosecond. The peak temperatures obtained at melanin will lead to thermomechanical damages. In addition, recent studies by Schuele²⁷ show that transition from thermal damage to thermomechanical damage occurs in the range of $50 \mu\text{s}$ pulse duration. Hence, in order to model photocoagulation accurately, a nonuniform

heat absorption model as shown by Thompson²⁸ could be used in conjunction with two phase models. Developing these models to evaluate thermomechanical effects is not a trivial task as it would require not only accounting of latent heat (using thermodynamic principles) but also phase change (multi-phase model) with formation and bursting of bubbles (interface tracking). To the author's knowledge such a complex multi-physics model does not exist at this time. This study is a base line numerical study, which could be improved upon with additional physics in the near future.

Further, uni-molecular chemical kinetics is not a suitable assumption for such high temperatures. Hence, the present study uses a uniform heat source assumption along with rate process analysis, to evaluate thermal damage caused by different laser parameters. Thus a more detailed analysis including two phase heat transfer should be developed to precisely predict the effect of laser parameters and is recommended for future work.

V. CONCLUSION

The laser tissue interaction during retinal treatment is analyzed to quantify thermal effects of variable laser parameters over selective damage of RPE using a numerical model of the eye. The results, based on Arrhenius integral value Ω , show both the area and magnitude of damage caused during the laser photocoagulation. Among different wavelengths, green laser is found to be more effective as it has high absorption in RPE. The damage caused by Gaussian profile shows selective damage along the radial direction. The beneficial effect of short-pulsed lasers over selectivity is explained using both instantaneous temperatures and Ω contours. The Ω contours show an increase in the area of damage with repetition frequency. The 100 Hz has better selective damage of RPE, while 1000 Hz produces more damage to the neural retina. The ratio of instantaneous temperatures $T_{\text{RPE}}/T_{\text{NR}}$, also shows the dissipation effects of higher frequency.

NOMENCLATURE

- A = frequency or pre-exponential factor (1/s)
- C = specific heat capacity (J/Kg K)
- E_a = activation energy (J/mole)
- f = laser frequency
- g = anisotropic factor
- I_0 = incident power of laser (W)
- k = thermal conductivity (W/m K)
- n = number of pulse
- r = radius (m)
- R = radius of the laser spot (m)
- R_u = universal gas constant – 8.32 (J/mole K)
- S = laser heat source (W/m^3)
- t = time (second)
- Δt_p = pulse duration (second)
- T = temperature (K)
- z = depth (m)
- ρ = density of tissue (kg/m^3)
- μ_a = absorption coefficient (1/m)

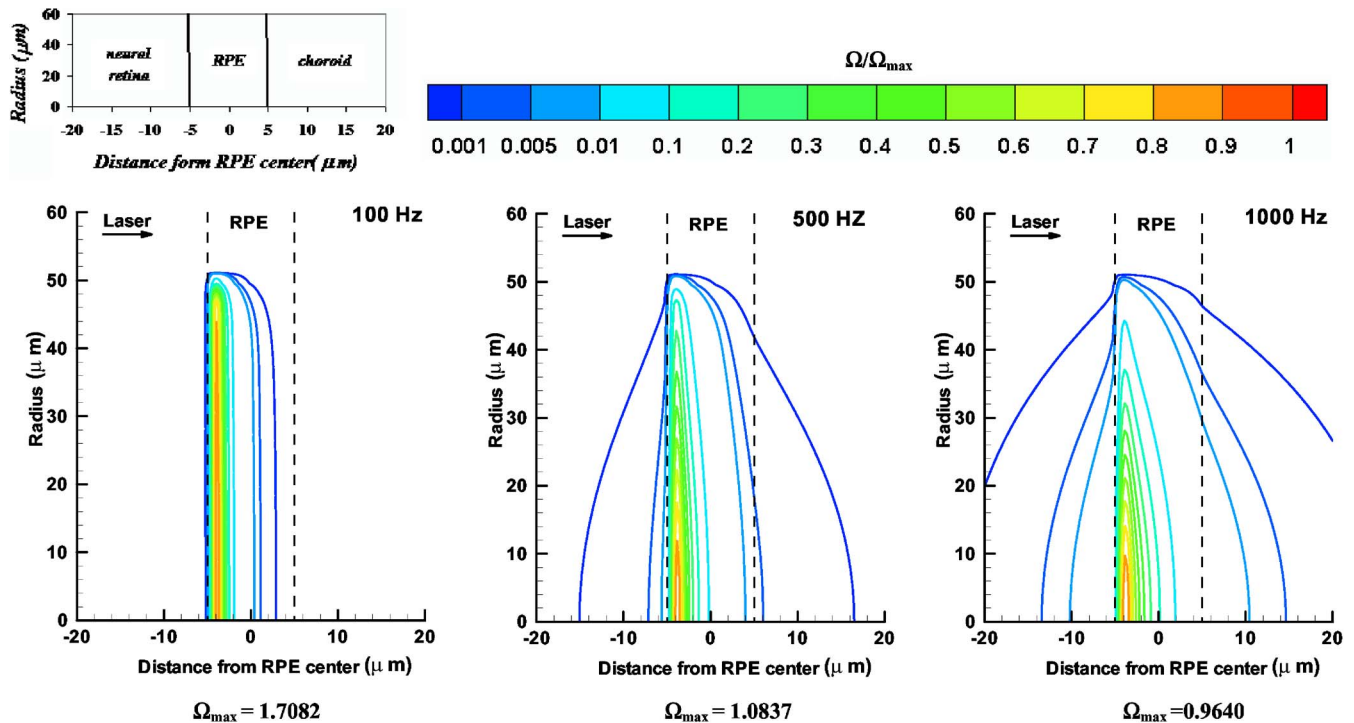


FIG. 11. Contours of Ω/Ω_{\max} for all repetition frequencies of 100, 500 and 1000 Hz. Frequency of 100 Hz produces selective damage to RPE, while 500 and 1000 Hz frequencies produce damage to neural retina.

μ_s = scattering coefficient (1/m)
 ϕ = fluence rate (W/m^2)
 Ω = Arrhenius integral value
 λ = laser wavelength (nm)

^{a)} Author to whom correspondence should be addressed. Electronic mail: rupak.banerjee@uc.edu

¹ J. Roider, R. Brinkmann, C. Wirebelauer, H. Laqua, and R. Bringruber, "Subthreshold (retinal pigment epithelium) photocoagulation in macular diseases: A pilot study," *Br. J. Ophthalmol.* **84**, 40–47 (2000).

² M. A. Mainster, "Decreasing retinal photocoagulation damage: Principles and techniques," *Semin Ophthalmol.* **14**, 200–209 (1999).

³ M. A. Mainster, "Wavelength selection in macular photocoagulation," *Ophthalmology* **93**, 952–958 (1986).

⁴ J. Roider, N. A. Michaud, T. J. Flotte, and R. Bringruber, "Response of retinal pigment epithelium to selective photocoagulation," *Arch. Ophthalmol. (Chicago)* **110**, 1786–1792 (1992).

⁵ J. Roider, R. Brinkmann, C. Wirebelauer, H. Laqua, and R. Bringruber, "Retinal sparing by selective retinal pigment epithelial photocoagulation," *Arch. Ophthalmol. (Chicago)* **117**, 1028–1034 (1999).

⁶ C. Framme, R. Binkmann, R. Bringruber, and J. Roider, "Autofluorescence imaging after selective RPE laser treatment in macular diseases and clinical outcome," *Br. J. Ophthalmol.* **86**, 1099–1106 (2002).

⁷ C. Framme, G. Schuele, J. Roider, R. Bringruber, and R. Brinkmann, "Influence of pulse duration and pulse number in selective RPE Treatment," *Lasers Surg. Med.* **34**, 206–215 (2004).

⁸ J. Roider, C. Lindermann, E. E. Hifnawi, H. Laqua, and R. Bringruber, "Therapeutic range of repetitive nanosecond laser exposures in selective RPE photocoagulation," *Graefes Arch. Clin. Exp. Ophthalmol.* **236**, 213–219 (1998).

⁹ J. Roider, E. E. Hifnawi, and R. Bringruber, "Bubble formation as primary interaction mechanism in retinal laser exposure with 200 ns laser pulses," *Lasers Surg. Med.* **22**, 240–248 (1998).

¹⁰ R. Brinkmann, G. Httmann, J. Rogener, J. Roider, R. Bringruber, and C. P. Lin, "Origin of retinal pigment epithelium cell damage by pulsed laser irradiance in the nanosecond to microsecond time region," *Lasers Surg. Med.* **27**, 451–464 (2000).

¹¹ J. W. Berger, "Thermal modeling of micropulsed diode laser retinal pho-

toagulation," *Lasers Surg. Med.* **20**, 409–415 (1997).

¹² M. W. Charles and N. Brown, "Dimension of the eye relevant to radiation protection," *Phys. Med. Biol.* **20**, 202–218 (1975).

¹³ E. H. Amera, "Numerical investigation on thermal effects of laser-ocular media interaction," *Int. J. Heat Mass Transfer* **38**, 2479–2488 (1995).

¹⁴ T. W. Olsen, S. Y. Aaberg, D. H. Geroski, and H. F. Edelhauser, "Human sclera: Thickness and surface area," *Am. J. Ophthalmol.* **125**, 237–241 (1998).

¹⁵ M. Hammer and D. Schweitzer, "Quantitative reflection spectroscopy at the human ocular fundus," *Phys. Med. Biol.* **47**, 179–191 (2002).

¹⁶ M. S. Stay, J. Xu, T. W. Randolph, and V. H. Barocus, "Computer simulation of controlled-release drugs in the vitreous humour," *Pharm. Res.* **20**, 96–102 (2003).

¹⁷ A. J. Welch, J. A. Pearce, K. R. Diller, G. Yoon, and W. F. Cheong, "Heat generation in laser irradiated tissue," *J. Biomed. Eng.* **111**, 62–68 (1989).

¹⁸ A. J. Welch and G. D. Polhamus, "Measurement and prediction of thermal injury in the retina of the rhesus monkey," *IEEE Trans. Biomed. Eng.* **31**, 633–644 (1984).

¹⁹ M. Hammer, A. Roggan, D. Schweitzer, and G. Muller Phys, "Optical properties of ocular fundus tissues – an in vitro study using the double-integrating- sphere technique and inverse Monte Carlo simulation," *Med. Biol.* **40**, 963–978 (1995).

²⁰ A. R. Moritz and F. C. Henriques, "Studies of thermal injury in the conduction of heat to and through skin and temperatures attained therein: A theoretical and experimental investigation," *Am. J. Pathol.* **23**, 915–934 (1947).

²¹ R. Bringruber, F. Hillenkamp, and V. P. Gabel, "Theoretical investigation of laser thermal injury," *Health Phys.* **48**, 781–796 (1985).

²² J. Pearce and S. Thomsen, "Rate process analysis of thermal damage," *Optical-Thermal Response of Laser-Irradiated Tissue*, edited by A. J. Welch and M. J. C. van Gemert (Plenum, New York, 1995), Chap. 17, pp. 561–603.

²³ A. N. Takata, L. Goldfinch, J. K. Hinds, L. P. Kuan, and N. Thomopoulos, "Thermal model of laser induced eye damage," Final Report, USAF School of Aerospace medicine, Brooks AFB TX, Contract No. F41609-74-C-0005, IIT Research Institute, Chicago, IL (1974).

²⁴ A. Mhaisekar, M. J. Kazmierczak, and R. K. Banerjee, "Steady conjugate heat transfer from laser or x-ray heated sphere in external flow at low

- Reynolds number ($Re=100$),” *Numer. Heat Transfer, Part A* **47**, 849–874 (2005).
- ²⁵A. Mhaisekar, M. J. Kazmierczak, and R. K. Banerjee, “Three dimensional numerical analysis of convection and conduction cooling of spherical biocrystals with localized heating from synchrotron x-ray beams,” *J. Synchrotron Radiat.* **12**, 318–328 (2005).
- ²⁶G. Schuele, C. Framme, J. Roider, and R. Brinkmann, “Noninvasive optoacoustic temperature determination at the fundus of the eye during laser irradiation,” *J. Biomed. Opt.* **9**, 173–179 (2004).
- ²⁷G. Schuele, M. Rumohr, G. Huettmann, and R. Brinkmann, “RPE damage thresholds and mechanism for laser exposure in the microsecond to millisecond time regimen,” *Invest. Ophthalmol. Visual Sci.* **46**, 714–719 (2005).
- ²⁸C. R. Thompson, B. S. Gerstman, S. L. Jacques, and M. E. Rogers, “Melanin granule model for laser-induced thermal damage in the retina,” *Bull. Math. Biol.* **58**, 513–553 (1996).